

# Security-Constrained Active Power Curtailment Considering Line Temperature and Thermal Inertia

Roman Bolgaryn<sup>1</sup>, Jan Wiemer<sup>1</sup>, Alexander Scheidler<sup>1</sup>, and Martin Braun<sup>2</sup>

<sup>1</sup>Fraunhofer Institute for Energy Economics and Energy System Technology IEE

<sup>2</sup>University of Kassel

June 12, 2023

## Abstract

We introduce a novel method to determine cost-optimized Active Power Curtailment (APC) of Renewable Energy Sources (RES) considering weather dependent Dynamic Line Rating (DLR). A new formulation of the Security-Constrained Optimal Power Flow (SC-OPF) is developed and applied in a case study. We demonstrate the reduction of the required preventive APC in the (N -0) case for (N -1) secure grid operation due to the consideration of thermal inertia of overhead power lines. Considering thermal inertia allows relying on curative APC that is activated only after an (N -1) situation occurs. The overhead power line temperature, calculated with the temperature dependent power flow, acts as a new limit for line loading and releases unused transmission reserves. The power system can be utilized to a greater extent, with a reduced demand for congestion management.

# Security-Constrained Active Power Curtailment Considering Line Temperature and Thermal Inertia

Roman Bolgaryn , Jan Wiemer , Alexander Scheidler, and Martin Braun 

We introduce a novel method to determine cost-optimized Active Power Curtailment (APC) of Renewable Energy Sources (RES) considering weather dependent Dynamic Line Rating (DLR). A new formulation of the Security-Constrained Optimal Power Flow (SC-OPF) is developed and applied in a case study. We demonstrate the reduction of the required preventive APC in the ( $N-0$ ) case for ( $N-1$ ) secure grid operation due to the consideration of thermal inertia of overhead power lines. Considering thermal inertia allows relying on curative APC that is activated only after an ( $N-1$ ) situation occurs. The overhead power line temperature, calculated with the temperature dependent power flow, acts as a new limit for line loading and releases unused transmission reserves. The power system can be utilized to a greater extent, with a reduced demand for congestion management.

**Index Terms**—Preventive and Curative Active Power Curtailment, ( $N-1$ )-security, Temperature Dependent Power Flow, Thermal Inertia.

## I. INTRODUCTION

TRANSMISSION System Operators (TSOs) commonly use Active Power Curtailment (APC) to mitigate grid congestion driven by the increasing amount of Renewable Energy Resources (RES). APC can be applied during contingency-free ( $N-0$ ) grid operation in such a way that it not only mitigates grid congestion in the ( $N-0$ ) case, but also prevents congestion in a case of an ( $N-1$ ) situation [1]–[3]. APC can be seen as preventive and curative. Preventive, or pre-fault, APC is applied in a contingency-free situation to avoid grid congestion if a contingency occurs and curative, or post-fault, APC is applied as a reaction on the contingency occurring [4], [5]. In this case, the curative measures are part of the grid operation strategy that avoids the breach of operational constraints rather than constitute the emergency response to an occurred breach of operational constraints. Since outages of transmission lines rarely occur, curative actions have the potential to reduce the need for cost-intensive preventive congestion management measures [4]. In this process, the direct consideration of the weather-dependent overhead power line temperature as a new, dynamic upper limit helps to avoid unnecessary APC and improves the utilization of the power system, because in favorable weather conditions, the lines can be utilized well above the static rating. Due to the effect of thermal inertia of conductors the final conductor temperature, after a change of a relevant parameter, is only reached after a certain time. This time delay can be exploited in a contingency situation. We define the time from the occurrence of a

contingency until a curative measure (in our case active power curtailment) is applied within a worst-case reaction time. If a faster reaction time is granted than the heating process of the conductor lasts, the grid can be utilized to a higher degree in the normal state. If a contingency situation occurs, the line starts to heat up and would end in a limit violation without the granted curative APC. The active power curtailment limits the final line temperature to its allowed limit.

We assume the situation in which RES cause grid congestion and APC is necessary to mitigate it, and propose a method to calculate preventive and curative APC that relies on Temperature-Dependent Power Flow (TDPF).

We propose a novel method that combines Temperature-Dependent Power Flow (TDPF) with Security-Constrained Optimal Power Flow (SC-OPF) using Linear Programming (LP) optimization to calculate both preventive and curative APC. By integrating these techniques, we can accurately determine the required preventive and curative APC for the given weather conditions and a guaranteed reaction time. Our novel method incorporates the weather dependency and thermal inertia directly into the optimization problem to obtain the curative Active Power Curtailment (APC). Our approach improves the utilization of the power system by accounting for the temperature-dependent limits of the power lines. We illustrate in a case study, for different weather conditions, how the guaranteed reaction time impacts the required preventive and curative APC.

In section II and section III of the paper, we provide an extensive review of literature to sufficiently introduce the approaches used in our work, and summarize relevant information we gathered while preparing this paper. We introduce the state of the art of the Active Power Curtailment (APC) and the Dynamic Line Rating (DLR). Afterwards, we describe the state of the art of the TDPF calculation and of SC-OPF using LP optimization. We describe the concepts of preventive and curative APC. Next, we describe our methodology approach of the implemented algorithm, and demonstrate it with a case study. In the end, we discuss the convergence properties and performance of our implementation.

The work of R. Bolgaryn, J. Wiemer, A. Scheidler, and M. Braun presents selected developments within the project “RobustPlan” (Grant No. 03EI6037B), funded by the German Federal Ministry for Economic Affairs and Climate Action (BMWK, formerly known as the German Federal Ministry for Economic Affairs and Energy), based on a decision of the Parliament of the Federal Republic of Germany. The authors are solely responsible for the contents of this publication. (Corresponding author: Roman Bolgaryn.)

R. Bolgaryn, J. Wiemer, and A. Scheidler are with the Division of Grid Planning and Operation, Fraunhofer Institute for Energy Economics and Energy System Technology, 34119 Kassel, Germany (e-mail: {roman.bolgaryn, jan.wiemer, alexander.scheidler}@iee.fraunhofer.de).

M. Braun is with the Department of Energy Management and Power System Operation, University of Kassel, 34121 Kassel, Germany, and also with the Division of Grid Planning and Operation, Fraunhofer Institute for Energy Economics and Energy System Technology, 34119 Kassel, Germany (e-mail: martin.braun@uni-kassel.de).

## II. ACTIVE POWER CURTAILMENT AND DYNAMIC LINE RATING

Conventionally, APC is applied based on static line ratings. The rated current serves as a limit to line loading and ensures that the line sag does not cause the breach of minimum clearances between the conductors of overhead power lines and the ground. Static line ratings are derived from worst-case weather assumptions defined in EN 50 341 [6]: the ambient air temperature of 35 °C, the wind speed (at a 90° angle to the conductor) of 0.6 m/s and the solar radiation of 900 W/m<sup>2</sup>. Electric losses increase the temperature of the conductors, leading to thermal expansion of the material of the conductors and an increase of the line sag. Common aluminum-steel conductors reach their maximum allowed sag at 80 °C, and this temperature limit, together with the worst-case weather assumption, defines the rated current of the conductor [7], [8]. The EN 50 182 standard, applicable to the design of overhead power lines in Europe, guides the calculation of the rated current.

An important aspect of additional loading limits must be considered. Line temperature is not the only relevant limit of the current carrying capacity of the electric circuit. For instance, protection devices, switch-gear, bus-bars, electromagnetic interference with parallel infrastructure etc. also limit the maximum current [5]. If the reaction time is very short, the current after a line outage can exceed such additional limits. It is possible that the thermal limit cannot be reached at all due to the mentioned additional limits. To account for this aspect, an additional current limit must be considered independently from overhead line temperature. We account for it by incorporating additional current limits in our method (section IV-B).

Alternatively, the required amount of APC can be reduced by using the actual temperature of overhead conductors as the capacity limit, if the actual weather conditions are known. In operation, the worst-case weather conditions are rarely observed, and oftentimes the lines would not reach their thermal limit even if their rated loading were exceeded. The Dynamic Line Rating (DLR) is calculated based on the line current and the observed weather conditions. Provided that weather conditions allow it, the line loading can be increased, as long as the maximum conductor temperature is not exceeded [9]. The physical limit of the maximum allowed temperature at observed weather conditions replaces the current limit derived from the maximum conductor temperature at worst-case conditions. Consequently, the need for preventive APC is reduced in operation during the times when the weather conditions are accommodative for higher line loading.

## III. TEMPERATURE-DEPENDENT POWER FLOW

To obtain the required APC under consideration of DLR it is necessary to consider the overhead power line temperature in the power system analysis. The best way to achieve it is the TDPF. In the following, we review the literature on TDPF in detail.

### A. Thermal models

The overhead power line temperature is defined by the processes of heating and cooling: Joule heating due to electric

losses and the absorption of solar radiation contribute to the increase of the line temperature, while the emitted thermal radiation and convection moderate it [10]. Equation (1) shows the steady-state heat balance for constant electrical conditions and constant weather conditions [9]. The term  $q_c$  describes the heat loss due to convection. The term  $q_r$  represents radiated heat loss and  $q_s$  describes the heat gain from the sun. The term  $I^2 \cdot R(T_{ss})$  represents the heat gain in the conductor due to electric losses, with the resistance of the conductor  $R(T_{ss})$  at the steady-state temperature  $T_{ss}$ .

$$q_c + q_r = q_s + I^2 \cdot R(T_{ss}) \quad (1)$$

There are two main mathematical models used in the industry to calculate overhead power line temperature and define the line rating [10]. Namely, the CIGRE model [11] and the IEEE model [9]. Both models enable the calculation of the steady state temperature that corresponds to the thermal balance of heating and cooling. Moreover, both models support to consider non-steady state calculation in time domain, e.g. after a sudden change of current flowing through the line.

### B. Inclusion of temperature in power flow calculation

A straightforward approach to consider line temperature in power flow calculation is a decoupled calculation [12]. The temperature model is combined with the power flow calculation in an alternating order, in which a correction of the resistance values occurs in between the sequential power flow calculations [13]. This approach has an advantage of the simplicity of implementation. However, it has a higher computational burden than the full integration within the Newton-Raphson power flow calculation. The AC power flow can be modified to include the line temperature in the state vector, along with voltage magnitude and voltage angle, to provide the line temperature as a direct result.

A modified Newton-Raphson method for Temperature-Dependent Power Flow (TDPF) calculation has first been introduced in [12]. To include the branch temperature in the calculation, several modifications were made to the power flow algorithm. First, the admittance matrix is updated at every iteration to consider changes in resistance based on the computed branch temperature. In addition, the state vector is expanded to include the branch temperatures. Moreover, the mismatch equations are expanded by the temperature difference. Most importantly, the Jacobian matrix is expanded to include additional sub-matrices of partial derivatives, which account for the inter-dependencies between the branch temperatures and other system variables.

The thermal model of overhead power lines is approximated through a thermal resistance constant  $R_\theta$ . It describes a linear dependence of the temperature rise  $T_{Rise}$  over the ambient temperature  $T_{amb}$  from the heat that is flowing out of the line i.e. power losses  $P_{Loss}$  (eq. (2)). The thermal resistance is defined for every overhead power line through the temperature rise and losses at the rated line loading, and remains constant throughout the calculation. Power losses serve as the connection between the power flow equations and line temperature in the power flow calculation.

$$R_{\theta} = \frac{T_{Rise}}{P_{Loss}} = \frac{T_{ss} - T_{amb}}{P_{Loss}} \quad (2)$$

$R_{\theta}$  is also defined for transformers and underground cables. Although this approach relies on simplified thermal models of power system components, it is so far, to the best of our knowledge, the only TDPF method that includes overhead power lines, cables and transformers at the same time.

The electrical resistance  $R$  of a power line depends on the temperature  $T$  as described by eq. (3), where  $R_{ref}$  is the reference resistance as found in a data sheet of the conductor, and  $T_{ref}$  is the reference temperature at which  $R_{ref}$  is valid (usually 20 °C). The temperature is changed at every iteration of the power flow calculation, making it necessary to also update the admittance matrix  $Y_{bus}$  at every iteration of the Newton-Raphson method.

$$R = R_{ref} \cdot (1 + \alpha \cdot (T - T_{ref})) \quad (3)$$

The temperature changes with every iteration because it is included in the state vector, and the mismatch vector is expanded to include temperature difference. This is shown in eq. (4) that describes the Newton-Raphson iteration of the power flow calculation. More precisely, it describes the calculation of a new guess for the state vector for the iteration  $k + 1$  from the previous guess at the iteration  $k$ , given the updated Jacobian matrix and the mismatch vector. It can be seen that the state vector includes line temperature  $T$  and the mismatch vector is expanded by temperature difference  $H$ .

$$\begin{bmatrix} \delta^{k+1} \\ V^{k+1} \\ T^{k+1} \end{bmatrix} = \begin{bmatrix} \delta^k \\ V^k \\ T^k \end{bmatrix} + (J^k)^{-1} \cdot \begin{bmatrix} \Delta P^k \\ \Delta Q^k \\ \Delta H^k \end{bmatrix} \quad (4)$$

In contrast to the active and reactive power set-points, temperatures of branches are not known, requiring temperature difference equations  $H$  to be defined as the difference between the values at the current iteration step and the calculated values. The eq. (5) describes the calculation of the temperature difference vector using  $R_{\theta}$  [12]. The terms  $T$ ,  $V$ , and  $\delta$  describe the value of the state vector and  $g(T)$  is the temperature-dependent value of branch conductance.

$$\begin{aligned} H_{ij}(\delta, V, T) = & T_{ij} - (T_{amb} + \\ & R_{\theta,ij} \cdot (g_{ij}(T) \cdot (V_i^2 + V_j^2) - \\ & 2g_{ij}(T) \cdot V_i V_j \cos(\delta_i - \delta_j))) = 0 \end{aligned} \quad (5)$$

Finally, the Jacobian matrix is expanded by additional sub-matrices of the partial derivatives of the active and reactive power, as well as the temperature difference, with respect to the line temperature (eq. (6)). The formulations of the sub-matrices of the Jacobian matrix are described in detail in [12].

$$J(\delta, V, T) = \begin{bmatrix} \frac{\partial P}{\partial \delta} & \frac{\partial P}{\partial V} & \frac{\partial P}{\partial T} \\ \frac{\partial Q}{\partial \delta} & \frac{\partial Q}{\partial V} & \frac{\partial Q}{\partial T} \\ \frac{\partial H}{\partial \delta} & \frac{\partial H}{\partial V} & \frac{\partial H}{\partial T} \end{bmatrix} \quad (6)$$

An implementation of TDPF that considers all the relevant weather parameters for overhead power lines exactly according to the IEEE model was presented in [14] as a further development from [12]. In contrast to [12], the IEEE thermal model is implemented completely rather than using a simplified linear approximation.

Both of the above methods do not consider thermal inertia, even though the IEEE model includes this possibility [9]. Namely, in an equivalent manner as the RC time constant, the time constant  $\tau$  defines the time that is required for the temperature to reach  $1 - e^{-1}$  ( $\approx 63\%$ ) of its steady state value. The calculation of non-steady state temperature eq. (8) relies on a linear approximation of radiative heat losses.

The method proposed in [15] incorporates the calculation of thermal inertia according to the aforementioned principle. The authors simplify the CIGRE model by linear approximation of some of the equations but still achieve a good trade-off between the calculation performance and the accuracy of the results. The approximate model includes a linear and a quadratic term of the relationship between the line losses and temperature (eqs. (7) and (8)).

$$T_{ss} = a_0 + a_1 \cdot I^2 + a_2 \cdot I^4 \quad (7)$$

$$T = T_{ss} - (T_{ss} - T_0) \cdot \exp(-t/\tau) \quad (8)$$

The model constants  $a_0$ ,  $a_1$ ,  $a_2$  describe the relationship between the temperature of overhead power lines and the current  $I$ , and the term  $\tau$  is the time constant. In the eqs. (7) and (8),  $T_{ss}$  stands for steady state temperature and  $T$  stands for the temperature that is reached after a reaction time  $t$  from the condition with the initial temperature  $T_0$ .

The deviations from the CIGRE model are within single digits K even for high conductor loading situations. The model was used to extend the MATPOWER [16] OPF to enable using overhead power line temperature directly as a constraint [10]. However, the temperature resulting from the calculation is not directly used to update the line resistance, and a sequential calculation of OPF and power flow is required to fully consider the effect of line temperature on resistance.

The AC power flow calculation using this model, with the general approach as in [12], [14], was extended by consideration of thermal inertia in [17] and for the first time allowed non-steady state calculations of overhead power line temperature directly in the Newton-Raphson power flow calculation. With this approach, two different TDPF calculations are possible: TDPF for steady-state temperature and Dynamic TDPF (DTDPF) for temperature rise from a given starting temperature after a set time delay.

### C. Our implementation in software

We provide the benefit to the community by releasing the method of TDPF and DTDPF used in this paper as part of the open-source Python library pandapower [18]–[21].

We use the approximate temperature model [15], [17] to consider weather data in our calculation. We then combine it with the method of [12] through calculation of the thermal

TABLE I  
ADDITIONAL INPUT PARAMETERS FOR THE TEMPERATURE MODEL

Parameter	Unit
Ambient air temperature	°C
Maximum rated temperature of overhead power lines	°C
Reference specific resistance	Ω/km
Conductor outer diameter	m
Specific heat capacity	J/(m K)
Wind speed	m/s
Angle between wind direction and conductor	°
Global solar radiation	W/m <sup>2</sup>
Temperature coefficient of resistance	1/K
Absorptivity factor	—
Emissivity factor	—

resistance  $R_{\Theta}$ . In particular, we modify the calculation of  $R_{\Theta}$  by combining eq. (2) and eq. (7) as shown in eq. (9).

$$R_{\Theta} = \frac{T_{Rise}}{P_{Loss}} = \frac{a_0 + a_1 \cdot I^2 + a_2 \cdot I^4 - T_{amb}}{P_{Loss}} \quad (9)$$

We update  $R_{\Theta}$  at every iteration of the Newton-Raphson algorithm rather than keeping it constant. Furthermore, we multiply the sub-matrices  $\frac{\partial H}{\partial \delta}$  and  $\frac{\partial H}{\partial V}$  by  $1 - \exp(-t/\tau)$  to include the thermal inertia in the Jacobian matrix, as in [15], [17]. We also modify the temperature mismatch equation by including the thermal inertia according to eq. (8). This enables a more accurate consideration of weather data and ensures the calculation results are in line with [15].

The input parameters that are necessary for the thermal model besides the grid data are summarized in Table I. The output of the TDPF algorithm, in addition to the outputs of the conventional power flow calculation, is the temperature of the overhead power lines, either steady state or non-steady state for a given time delay. The resistance values are adjusted within the TDPF calculation (eqs. (3) and (4)) and all the results are valid for the resistance values that match the calculated temperature.

#### IV. SECURITY-CONSTRAINED TEMPERATURE-DEPENDENT OPTIMAL POWER FLOW

APC is employed to ensure the grid operates within its operational limits. However, APC incurs costs due to the lost revenue of operators of the generators. In some regulatory regimes, the grid operators are obligated to compensate these costs, but this is not the case everywhere. This question is not in the scope of this paper, because we consider the overall macroeconomic costs of APC rather than the costs incurred by individual parties. To avoid excessive costs of APC, optimization techniques can be applied that try to minimize the costs of APC while satisfying the operational constraints.

To obtain the required APC under consideration of DLR and thermal inertia we implement two methods of OPF using a linear programming (LP) approach. In the following, we first introduce the state of the art of OPF calculation using LP in AC domain. Afterwards, we describe our innovation to combine TDPF and OPF - TDOPF. Finally, we introduce the method of Security-Constrained Dynamic Temperature-Dependent OPF (SC-DTDOPE) that can be utilized for calculation of preventive APC.

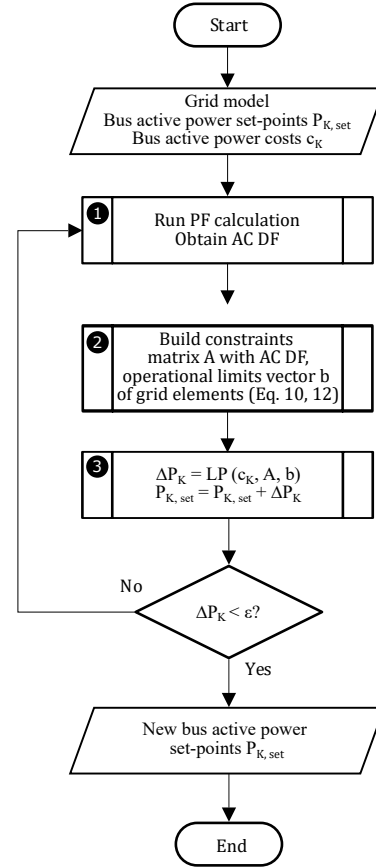


Fig. 1. State of the art optimal power flow with AC distribution factors [23]

##### A. State of the art of AC OPF using LP

Power flow calculation with the Newton-Raphson method solves the non-linear power flow equations. Along with the results for bus voltages and branch power flows, the power flow calculation determines a valid grid operational point with the established power balance. In addition, a valuable byproduct of this calculation is the Jacobian matrix: it contains information about the linear dependency of bus active and reactive power injections on the bus voltage magnitude and angle. The inverse of the Jacobian matrix provides the AC distribution factors for the bus-related quantities.

Linear approximation is a means to simplify the otherwise non-linear mathematical problem of the AC OPF. To this end, we use AC distribution factors for bus voltage and branch current that enable us to define the LP optimization problem. Linear programming is a commonly used way to formulate OPF problems [1]–[3], [22], [23].

In this paper, we build upon our previous work in [23] where we introduced an AC OPF calculation method using LP optimization that satisfies the constraints of line current limits. This method consists of the following three basic steps that are repeated until a given convergence criterion is satisfied (fig. 1). In the first step of the algorithm, an AC power flow calculation is executed. The second step determines the constraints matrix  $A$  for the LP problem via the AC distribution factors for the given grid state, and the operational limits vector  $b$  that defines the minimum and maximum limits for bus voltage and line

current. The third step solves the LP problem and updates the bus power injections based on the solution of the LP problem: the changes of the injections  $\Delta P_K$  at every bus  $K$  are added to the previous set points of the generators. Finally, if the difference of the bus injections is below the set tolerance, the results of the last iteration are saved and the algorithm stops.

AC distribution factors provide the basis for this method. The branch admittance matrix allows to calculate the branch-related distribution factors that describe the linear dependency between branch power flows and bus power injections [2], [22]. In addition, the dependency of the current through branch  $ft$  on the power injection at bus  $K$   $DF_{I_{ft}} = \frac{dI_{ft}}{dP_k}$  can be obtained by applying the chain rule, as described in more detail in [23]. The values of the so defined AC distribution factors are valid at or close to the operational point of the converged AC power flow. An adjustment of the operational point by applying the solution of the LP problem renders the DF inaccurate. It is therefore necessary to apply a sequential procedure that repeats solving the power flow and the LP problem several times until the solution matches the operational point of the grid.

$$\begin{aligned}
& \text{minimize} && \sum (c_K^T \cdot \Delta P_K) \\
& \text{subject to} && V_K - DF_{V_K} \cdot \Delta P_K \leq V_{max,K} \\
& && V_K - DF_{V_K} \cdot \Delta P_K \geq V_{min,K} \\
& && I_{ft} - DF_{I_{ft}} \cdot \Delta P_K \leq I_{max,ft} \\
& && I_{ft} - DF_{I_{ft}} \cdot \Delta P_K \geq -I_{max,ft} \\
& && 0 \leq \Delta P_K \leq P_{max,K} \\
& && \forall ft \in L, \forall K \in B
\end{aligned} \tag{10}$$

To include the maximum and minimum constraints for voltage magnitude, we define the distribution factors matrix for the bus voltage magnitude  $DF_{V_K}$  using the sub-matrix  $\frac{\partial V}{\partial P}$  from eq. (11). In a similar manner, reactive power control can be implemented by using the sub-matrix  $\frac{\partial V}{\partial Q}$ . Voltage control via reactive power is out of the scope of this paper and we have not included it in our problem formulation. Similarly, the ramp constraints of the generators are not considered in the scope of the paper.

Equation (10) presents the LP problem. The vector  $c_K$  stands for the costs of the APC for every bus  $K$  from the set of all grid buses  $B$ . The vector  $\Delta P_K$  is the result of solving the LP problem: it denotes the change in active power injection or consumption for every bus  $K$ . The constraints for voltage are defined for every bus  $K \in B$  and the constraints for current are defined for every line  $ft$  from the set of all lines  $L$ . In practice, the sets  $B$  and  $L$  can be sub-sets of selected relevant buses and lines. The limits for the minimum  $\Delta P_{min,K}$  and the maximum  $\Delta P_{max,K}$  change of the active power are calculated based on the minimum and maximum limits of the generators and the current set-points of the active power.

The LP problem is solved with the Python library SciPy [24] that implements the method described in [25].

## B. Temperature-Dependent Optimal Power Flow

The implementation of TDPF i.e. obtaining the overhead power line temperature as a direct result of the Newton-Raphson power flow calculation allows using it as a variable in AC OPF. More precisely, the inverse of the Jacobian matrix (eq. (11)) contains the AC distribution factors  $\frac{\partial T}{\partial P}$  describing the linear approximation of the dependence of the overhead line temperature from the bus active power injections.

$$J(\delta, V, T)^{-1} = -1 \cdot \begin{bmatrix} \frac{\partial \delta}{\partial P} & \frac{\partial \delta}{\partial Q} & \frac{\partial \delta}{\partial H} \\ \frac{\partial V}{\partial P} & \frac{\partial V}{\partial Q} & \frac{\partial V}{\partial H} \\ \frac{\partial T}{\partial P} & \frac{\partial T}{\partial Q} & \frac{\partial T}{\partial H} \end{bmatrix} \tag{11}$$

Because the distribution factors for overhead power line temperature are available from the Jacobian matrix after executing the TDPF, we can expand the LP formulation to define the Temperature-Dependent OPF (TDOPF) as shown in eq. (12).

$$\begin{aligned}
& \text{minimize} && \sum (c_K^T \cdot \Delta P_K) \\
& \text{subject to} && V_K - DF_{V_K} \cdot \Delta P_K \leq V_{max,K} \\
& && V_K - DF_{V_K} \cdot \Delta P_K \geq V_{min,K} \\
& && T_{ft} - DF_{T_{ft}} \cdot \Delta P_K \leq T_{max,ft} \\
& && T_{ft} - DF_{T_{ft}} \cdot \Delta P_K \geq -T_{max,ft} \\
& && I_{ft} - DF_{I_{ft}} \cdot \Delta P_K \leq I_{max,ft} \\
& && I_{ft} - DF_{I_{ft}} \cdot \Delta P_K \geq -I_{max,ft} \\
& && 0 \leq \Delta P_K \leq P_{max,K} \\
& && \forall ft \in L, \forall K \in B
\end{aligned} \tag{12}$$

To account for the loading limits that are independent from temperature (switch-gear limits etc.), the maximum current  $I_{max,ft}$  must be defined according to the limitations not related to the thermal rating of overhead power lines and included as a constraint of the LP problem. This limit is different than the current limit in eq. (10) because it is motivated by additional limits mentioned above instead of the rating of the line.

We expand the LP problem to incorporate line temperature by using the maximum allowed temperature of overhead power lines as constraints. The method relies on using the DF matrix obtained from the inverse of the Jacobian matrix after a successful convergence of TDPF, as shown in eq. (11). The inverse sub-matrix  $\frac{\partial T}{\partial P}$  has the dimensions of (number of branches)  $\times$  (number of buses - 1) and each element of it describes the change of line temperature at a particular line resulting from an incremental change of active power injection at a given bus. We use the sub-matrix  $\frac{\partial T}{\partial P}$  as the DF matrix to define the LP problem. In addition to the line temperature constraints, the line current and bus voltage constraints are included, as presented in eq. (12). The objective is to find a cost-optimized vector of APC  $\Delta P$  that satisfies the constraints. It is important to note that the problem formulation in eq. (12) refers to the LP programming part of the method. Because the

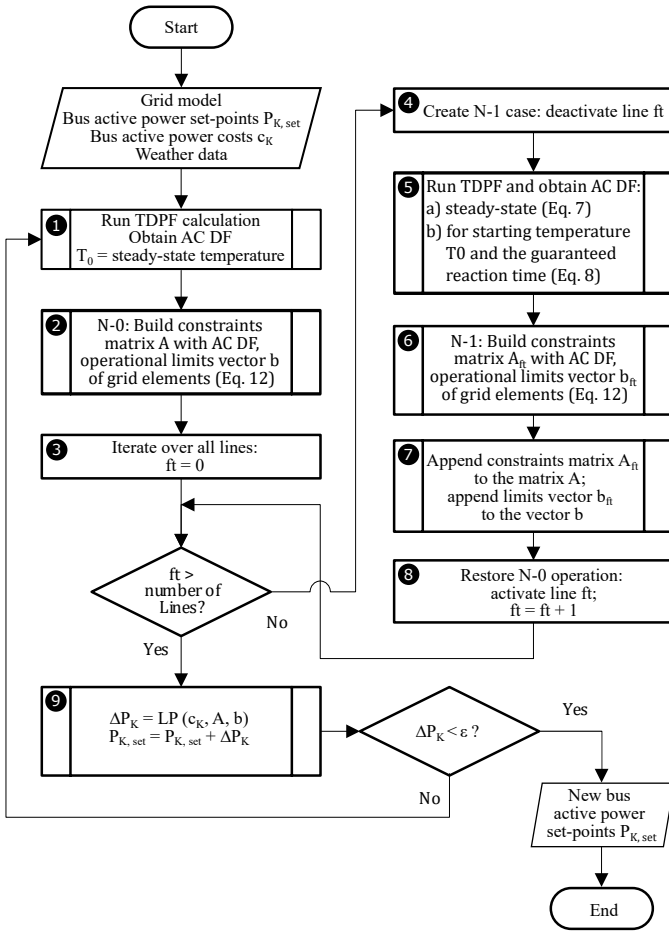


Fig. 2. The algorithm of security-constrained optimal power flow

power balance is restored by TDPF, including the power flow equations in the optimization problem is not necessary.

The algorithm of TDOPF is still the iterative process described in fig. 1, except that the first step is the solution of TDPF. The LP problem and the power flow calculation are solved repeatedly, until the difference between the LP solutions is below a set tolerance. The TDPF updates the values of line temperature and resistance, so that the resistance of lines is aligned with the line temperature every time the power flow calculation is executed. The power flow calculation restores the power balance, either via a single slack bus or with the distributed slack approach, updates the results for buses and branches, and provides the updated Jacobian matrix for the operational point defined by the previous solution of the LP problem. This approach requires a successfully converged TDPF, which is not always guaranteed. We discuss this issue additionally in section VII.

The TDOPF does not include any  $(N-1)$  contingencies, and the DF for line temperature are defined based on the TDPF solved for steady-state line temperature.

### C. Security Constrained Dynamic Temperature-Dependent Optimal Power Flow

Steady-state security of a power system is the ability of the system to operate within the specified limits following a

contingency [26]. If a possible contingency situation would lead to a violation of the specified limits, the steady-state security of the power system must be restored by modifying its contingency-free operation. Security-Constrained Optimal Power Flow is a method to obtain a cost-optimal change of bus power injection or consumption that is required to restore the steady-state security.

In contrast to OPF, the implementation of the SC-OPF must take into account not only the  $(N-0)$  but also all the  $(N-1)$  grid states. To this end, in our case a single potentially very large LP is formulated that includes the constraints of the  $(N-0)$  and all the  $(N-1)$  cases.

As we aim to obtain the APC with consideration of thermal inertia, we define the Security-Constrained Dynamic Temperature-Dependent OPF (SC-DTDOF). For every  $(N-1)$  case, the calculation of TDPF is replaced by the DTDPF that is based on a given guaranteed reaction time. This way, the resulting DF consider thermal inertia of the overhead power lines and the limit for the reaction time of the grid operator to engage additional APC. After the result of SC-DTDOF is obtained, TDOPF must be applied to every  $(N-1)$  situation separately to obtain the required APC to mitigate the post-contingency limit violations.

The inclusion of the guaranteed reaction time in the Jacobian matrix within the DTDPF calculation allows obtaining the DF through the power flow calculation. The constraints are defined with the use of the DF for the situation after a given reaction time (instead of the steady state) after the  $(N-1)$  event. The algorithm for the SC-DTDOF is introduced in fig. 2. The step 5 of the algorithm defines whether the algorithm applies to the steady-state overhead power line temperature (a - SC-TDOF (eq. (7)), or b - SC-DTDOF (eq. (8))).

First, we initialize the values of the steady state starting temperature  $T_0$  in  $(N-0)$  operation by means of a TDPF calculation (step 1). Next, we determine the matrix of constraints  $A$  that consists of the constraints matrices for voltage, temperature and current for the  $(N-0)$  situation, based on the distribution factors. The vector of operational limits  $b$  is defined according to the limits of bus voltage, line current and line temperature (step 2). The constraints are expanded to include the  $(N-1)$  situations in a loop, starting with the first line, which is the line with the index 0 (step 3). The line is set out of service to simulate an  $(N-1)$  contingency (step 4). The TDPF calculation is executed, and this step defines whether the algorithm obtains preventive-only APC without any consideration of curative measures (a) or the preventive APC assuming fast curative measures that can be activated within the guaranteed reaction time to exploit thermal inertia (b) with the starting value of  $T_0$  (the result of the contingency-free steady-state calculation from step 1) (step 5). The constraints for the contingency situation  $A_{ft}$  are defined based on the TDPF results and the distribution factors. The operational limits vector  $b_{ft}$  is defined according to the  $(N-1)$  limits of the grid elements (step 6). Next, the constraints matrix  $A$  is expanded by the constraints matrix  $A_{ft}$ , and the operational limits vector  $b$  is expanded by  $b_{ft}$  (step 7). Finally, the line is set back in service and the next line is selected for simulating the contingency situation (step 8). After all the

possible ( $N-1$ ) cases are simulated, the constraints matrix  $A$  and operational limits vector  $b$  are complete, the vector of APC  $\Delta P$  that is required to satisfy the constraints in the ( $N-0$ ) operation and all the ( $N-1$ ) situations is obtained by solving the LP problem. The set-points of generators are updated to include the APC (step 9). This process is repeated until the required change of the set-points of generators is negligible.

We define SC-DTDOFP with an LP model in eq. (13) that includes all the ( $N-1$ ) situations  $s$ . This allows to obtain the required change of bus power injection so that the line temperature limits are not exceeded either in the ( $N-0$ ) operation, nor in any of the possible ( $N-1$ ) situations, under consideration of the possibility to apply additional APC within a guaranteed reaction time (assuming fast curative measures).

$$\begin{aligned}
 & \text{minimize} && \sum (c_K^T \cdot \Delta P_K) \\
 & \text{subject to} && V_{K,s} - DF_{V_{K,s}} \cdot \Delta P_K \leq V_{max,K} \\
 & && V_{K,s} - DF_{V_{K,s}} \cdot \Delta P_K \geq V_{min,K} \\
 & && T_{ft,s} - DF_{T_{ft,s}} \cdot \Delta P_K \leq T_{max,ft} \\
 & && T_{ft,s} - DF_{T_{ft,s}} \cdot \Delta P_K \geq -T_{max,ft} \quad (13) \\
 & && I_{ft,s} - DF_{I_{ft,s}} \cdot \Delta P_K \leq I_{max,ft} \\
 & && I_{ft,s} - DF_{I_{ft,s}} \cdot \Delta P_K \geq -I_{max,ft} \\
 & && \Delta P_{min,K} \leq \Delta P_K \leq \Delta P_{max,K} \\
 & && \forall ft \in L, \forall K \in B, \forall s \in S
 \end{aligned}$$

The LP problem is defined for multiple situations  $s$  from the set of all grid situations  $S$  at the same time. The total number of  $s$  equals the number of lines  $|L|$  for the number of the ( $N-1$ ) situations plus 1 for the ( $N-0$ ) situation:  $|S| = |L| + 1$ . The matrix of line constraints does not include any inactive lines, therefore a matrix for constraint inequality for current or temperature includes  $|L| \cdot (|L| - 1) + |L|$  rows. For a voltage inequality matrix, the number of rows equals  $(|L| + 1) \cdot |B|$  where  $|B|$  is the number of buses. Every constraint variable (current, temperature and voltage) is represented by a pair of inequality matrices. Therefore, the total number of rows in the total constraints matrix is  $4 \cdot |L|^2 + 2 \cdot (|L| + 1) \cdot |B|$ . There are  $|B|$  columns in the constraints matrix.

## V. PREVENTIVE AND CURATIVE ACTIVE POWER CURTAILMENT

Preventive APC is applied in contingency-free ( $N-0$ ) operation to mitigate grid congestion in ( $N-0$ ) operation and to prevent grid congestion from occurring as a result of any possible ( $N-1$ ) contingency. With preventive APC, a contingency situation of any single line falling out of service does not lead to inadmissible loading of any line in the grid. In other words, a failure of any of the lines must not cause inadmissible overloading of the remaining lines. With only preventive APC, even if no further action by the grid operator occurs as a reaction to an ( $N-1$ ) situation, all lines remain within their admissible loading limits. With the use of DLR, the temperature of overhead power lines serves as the limit of line loading. In conservative ( $N-0$ ) operation,

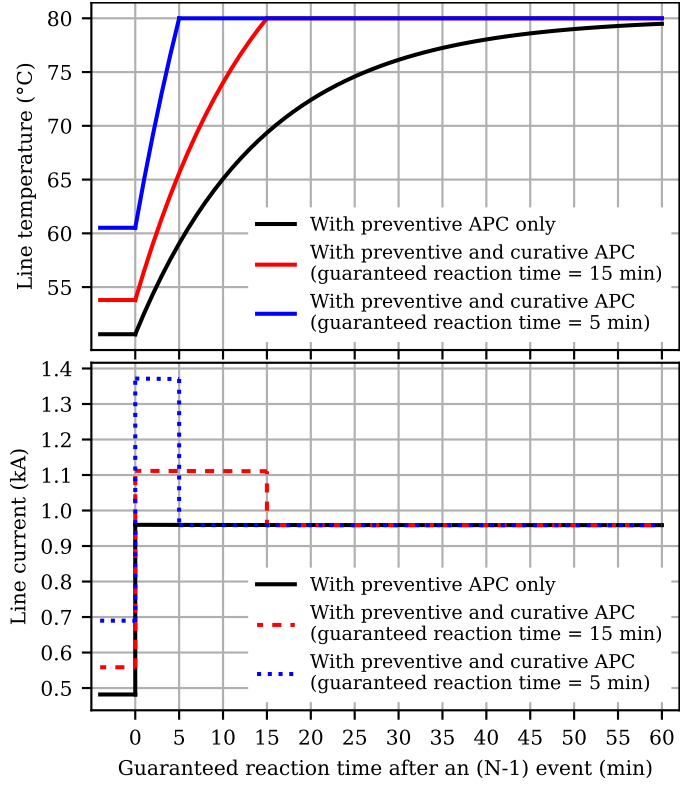


Fig. 3. Thermal inertia enables use of curative APC and a reduction of preventive APC, leading to a higher maximum line loading in ( $N-0$ ) operation

the line loading is reduced to the extent that any possible line outage does not lead to inadmissible line temperature in thermal steady-state. The steady state temperature in any of the ( $N-1$ ) cases determines the required amount of APC in the ( $N-0$ ) operation. The temperature limit is maintained by preventively limiting the power injection in anticipation of possible ( $N-1$ ) situations.

Thermal inertia provides reserves in grid operation. For instance, in the event of a line outage, the current flowing through the intact lines surges immediately. At the same time, the temperature of overhead power lines starts increasing. However, a certain time is required until the line temperature reaches its peak value corresponding to the steady state thermal balance. Due to thermal inertia, there is a time gap between the ( $N-1$ ) event and the maximum temperature rise, during which the TSO can activate additional, curative APC and reduce the line loading and stop the temperature from rising any further [5], [9], [17]. If APC can be activated (change of power dispatch is applied in the grid) within a guaranteed reaction time, before the line temperature reaches its corresponding limit, the preventive APC can be reduced due to the availability of the curative APC. The shorter this guaranteed reaction time, the higher the line utilization in normal operation can be maintained.

The following two conditions are necessary for curative APC: first, a short-term increase of the line loading limits is possible due to thermal inertia of conductors and second, the grid operator can activate additional APC within a predefined guaranteed reaction time after the ( $N-1$ ) situation. As a result

of this strategy, curative APC is activated after an  $(N-1)$  event occurred, and enables a reduction of the required preventive APC, leading to an increase of the grid loading and utilization in the  $(N-0)$  operation. We demonstrate this effect in a schematic illustration of the line temperature rise after a line outage in fig. 3. The temperature limit is set to  $80^\circ\text{C}$ . An  $(N-1)$  event happens at the time point 0, after which the current in the observed line increases immediately. However, the increase of the temperature of the line due to the increase of the electric losses is delayed because of the thermal inertia of the conductors.

When only considering preventive APC, the line temperature gradually increases until it reaches a steady state value of  $80^\circ\text{C}$  after approximately 60 min. Operating the power system below its capacity in the  $(N-0)$  condition is necessary to ensure that the temperature limit is not exceeded in any  $(N-1)$  situation. The required preventive APC in  $(N-0)$  operation is determined based on the steady state temperature in  $(N-1)$  situation and remains unchanged after the  $(N-1)$  event.

If curative curtailment is considered and activated within the reaction time of 15 min or less, the APC in the  $(N-0)$  operation is determined by the non-steady state temperature in the  $(N-1)$  situation. Allowing for higher line loading in the  $(N-0)$  operation and maintaining a higher line temperature leads to less preventive APC. The combined application of preventive and curative APC is illustrated with the red line in fig. 3 (above). Once the  $(N-1)$  event occurs, the current increases to a value higher than in the preventive APC only scenario. The  $80^\circ\text{C}$  thermal limit is reached after 15 min and would be exceeded afterwards. As long as curative APC is activated within 15 min the line temperature does not exceed the limit. The dynamic thermal balancing process is interrupted and a new thermal balance is established at the temperature of  $80^\circ\text{C}$  and maintained throughout the considered time span. Considering curative APC along with preventive APC allows for higher line loading in the  $(N-0)$  situation.

A shorter reaction time provides increased grid utilization by reducing the reaction time from 15 min to 5 min, as illustrated with the blue line in fig. 3. Although the current after the  $(N-1)$  event is higher, causing a faster temperature rise, the temperature limit is maintained due to the shorter guaranteed reaction time of curative APC. This results in reduced preventive APC requirements during  $(N-0)$  operation and improved grid utilization.

To obtain the required amount of curative APC, it is necessary to first apply the required preventive APC to establish the  $(N-0)$  grid state. Next, every  $(N-1)$  state is simulated separately, for which its respective curative APC is obtained.

## VI. CASE STUDIES

We demonstrate the proposed method of SC-OPF under consideration of line temperature and thermal inertia in a case study of an example power system derived from the PJM 5-bus system [27], [28]. We modified the power values of the synchronous generators and added a static generator to create a challenging scenario. Furthermore, we defined the power lines according to the standard line type "490-AL1/64-ST1A 220.0" [8]. The line length corresponds to the ratios

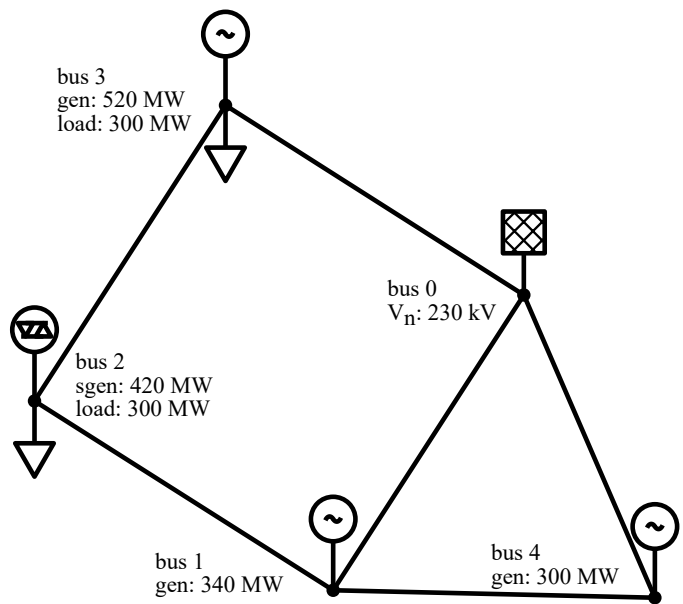


Fig. 4. The example grid used in the case study

TABLE II  
CASE STUDY: PARAMETERS FOR  $(N-0)$  AND  $(N-1)$  OPERATION

Parameter	Value
Solar radiation	$900 \text{ W/m}^2$
Absorptivity factor	0.5
Emissivity factor	0.5
Air temperature	$35^\circ\text{C}$
Max. line temperature	$80^\circ\text{C}$
Wind speed	$0.6 \frac{\text{m}}{\text{s}}; 1 \frac{\text{m}}{\text{s}}; 2 \frac{\text{m}}{\text{s}}$
Wind direction	$90^\circ$
Start temperature, $(N-1)$ cases	$(N-0)$ calculation results
Guaranteed reaction time, $(N-1)$ cases	5 min to 60 min

of reactance of the original lines and the specific reactance according to the used standard type. The scheme of the grid with the specified power values of generators and loads is presented in fig. 4. The outer diameter of the conductors is equal to 24.98 mm and the specific heat capacity is equal to  $1490 \text{ J/(m K)}$ . The costs of active power of all generators are set to equal values of  $-100 \text{ €/MWh}$ . Further assumptions are included in table II. In real life application, these parameters should be selected according to the installed grid assets and the weather measurements or weather forecasts. This information enables the reader to reproduce the grid we use in the case study.

The effect of the wind speed and the overhead power line temperature in SC-OPF is presented in table III (thermal inertia is not considered here). The first row represents the necessary APC when the line temperature is not considered. This value is very close to the APC obtained for the wind speed of  $0.6 \frac{\text{m}}{\text{s}}$  because this wind speed and the other weather parameters match the worst-case definition of EN 50 341, used to define the maximum loading limit. With higher wind speed values, the convective cooling of the lines increases and a reduction of the necessary APC can be observed. A practical use case is the application of DLR based on measured wind speed. In

TABLE III  
SC-OPF WITH AND WITHOUT TDPF

Wind speed	APC	Reduction of APC
—	264 MW	—
0.6 $\frac{m}{s}$	263 MW	0.34 %
1 $\frac{m}{s}$	196 MW	25.7 %
2 $\frac{m}{s}$	90.5 MW	65.7 %

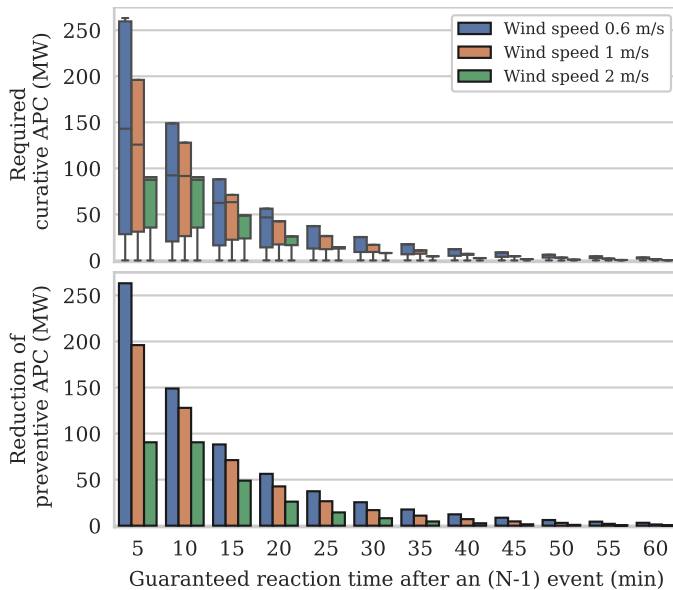


Fig. 5. Study A: curative APC as a reaction to  $N-1$  situations (upper figure) allows reducing preventive APC during  $N-0$  operation (lower figure). Shorter guaranteed reaction time enables more reduction of preventive APC.

the following, we add the consideration of thermal inertia to the case study.

When thermal inertia is considered, it is necessary to define the initial grid conditions and the initial line temperature. To this end, we define the power injections of generators according to an SC-TDOPF calculation with the temperature limit for the steady-state temperature of  $80^\circ\text{C}$ . This represents the reference case of only using preventive APC. Generation in the ( $N-0$ ) case is curtailed so that in case of any line outage the temperature of all lines remains below  $80^\circ\text{C}$ . The line temperature in the so defined ( $N-0$ ) condition serves as the initial temperature value for all further calculations.

#### A. Impact of wind speed on preventive and curative APC

The TDPF calculations are set up according to the weather data summarized in Table II. The weather parameters are defined in line with the worst-case assumptions in EN 50 341 [6]. In addition, we consider alternative wind speed values of  $1\text{ m/s}$  and  $2\text{ m/s}$  to demonstrate the effect of different weather conditions on the required APC. Table II summarizes the parameters for the ( $N-0$ ) and ( $N-1$ ) calculations in the case study. The degree of freedom of the SC-DTDOF is the reduction of power injection of the synchronous generators and the static generator. The power balance is restored by the slack bus.

We showcase the potential of curative APC to reduce the required preventive APC at different guaranteed reaction times in fig. 5. In the lower part of the plot, the bars represent the achieved reduction in required preventive APC. This reduction is a permanent benefit of the consideration of thermal inertia and of the guaranteed reaction time. Note that coincidentally the bars at 5 min mark represent the total required preventive APC, and so does the column “APC” in table III.

The reduction of the preventive APC is enabled by the curative APC, shown in the upper part of the plot. There are a total of 6 lines, yielding possible 6 ( $N-1$ ) situations. The value of the required curative APC depends on the particular ( $N-1$ ) situation. This is the reason why the curative APC is shown with a box plot. For instance, 2 of the ( $N-1$ ) situations do not lead to any additional APC beyond what is applied preventively. In the worst case, the entire reduction of the preventive APC must be activated as curative APC within the set guaranteed reaction time. In contrast to the permanent benefit through the reduction of the necessary preventive APC, the costs of the curative APC are only inflicted in the rare case of an ( $N-1$ ) situation actually occurring. Even then, the costs differ based on the severity of the actual ( $N-1$ ) case.

The wind speed has a high impact on the line temperature, which manifests itself in the observed differences of APC for the respective values of wind speed. This effect underlines the importance and the potential benefits for the grid operators to consider weather data in grid operation and grid planning. For instance, in situations of higher wind speed and possibly higher wind power output, it is possible that no preventive APC is required at all. In particular, with the wind speed of  $2\text{ m/s}$  in this case study, no preventive APC is necessary with the guaranteed reaction time of 10 min or less. Ignoring weather data in such a situation leads to unnecessary APC.

The variation of the guaranteed reaction time demonstrates the potential to reduce preventive APC if the grid operator has the ability to activate curative APC within a guaranteed time after an occurrence of an ( $N-1$ ) event. In this case study, the ability to activate curative APC within the first 5 min after an ( $N-1$ ) event eliminates the need for preventive APC entirely. A guaranteed reaction time of 10 min and 15 min, if applied as a buffer time for the human operator to react in case of a failed automatic dispatch, still leads to substantial reductions of the required preventive APC.

The reductions of preventive APC are enabled by the assumption that all of the required curative APC can be activated within the guaranteed reaction time. For the short reaction time values, this can present a limitation of the method due to the ramp constraints of generators. We are not addressing this limitation in this paper.

#### B. Relevance of the current constraints

We perform an additional case study to demonstrate the effect of including the line current as a constraint. We limit the line loading to 160% of the rated current. To achieve a situation when this additional current limit is relevant, we increase the power injection limit of generators by 25%. The elevated current limit serves as an additional safety margin

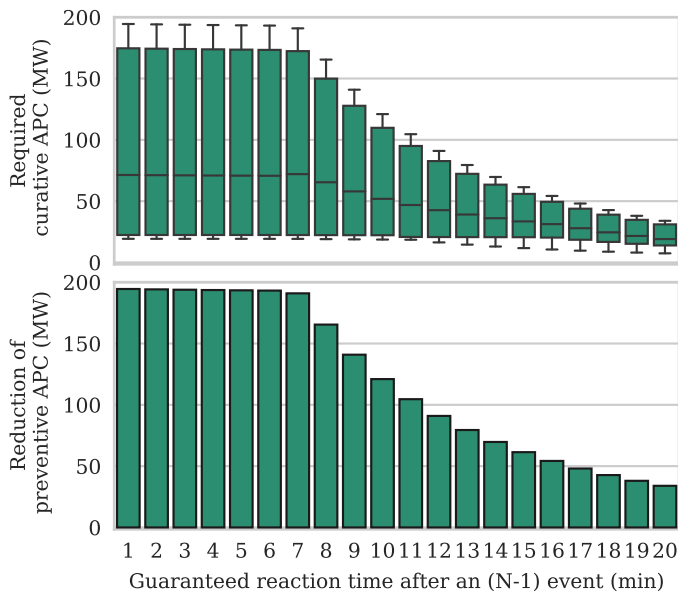


Fig. 6. Study B: The additional limit of the current increase leads to a cap of the benefit for all response times below 8 min

to account for other equipment in the grid (e.g. switch-gear equipment, bus-bars, protection relays etc.) or other reasons for limiting the current (e.g. electromagnetic interference, noise etc.). In case studies of real grids, this value should be selected based on the actual limits in question. We calculate the preventive and curative APC for this adjusted case study for the guaranteed reaction times up to 20 min with the time resolution of 1 min (fig. 6). We perform the calculation for the wind speed of 2 m/s.

The preventive APC does not increase for the first 7 values of the guaranteed reaction time because the relevant constraint during the first 7 min is the current limit. Eventually, as the guaranteed reaction time surpasses 7 min, line temperature becomes the relevant constraint. The attainable reduction of the preventive APC decreases, and the results have a similar trend as the results in the first case study. In other words, very short reaction times are likely to be limited by current limits rather than temperature limits, and rather generous guaranteed reaction time of 10 min to 15 min is enough to benefit from thermal inertia. In such circumstances, the backup plan can be implemented by having a human operator monitor the automatic calculations based on the given ( $N-1$ ) situation and intervene as required.

As a side note, we compare the power flow calculation with temperature consideration (TDPF) and without it (PF). Figure 7 represents the lines of the grid from the case study that matches the grid condition in fig. 6 with line temperature in the steady-state condition. It shows the difference between line loading and line resistance in percent, as well as the temperature of every line. It can be seen that depending on the ( $N-1$ ) case, the difference in line losses can reach close to 40%. The change in resistance is in two-digit percent range. Even a difference in the loading of lines can be observed in a lower single-digit percentage range. This demonstrates that considering TDPF is relevant for the accuracy of the results.

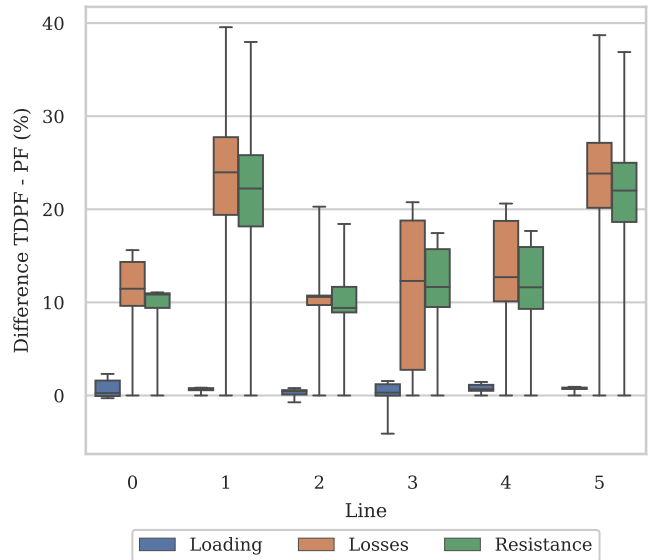


Fig. 7. Results difference between TDPF and PF, per line in %. Box plots represent variations due to the ( $N-1$ ) cases

## VII. STRATEGIES FOR CONVERGENCE

The proposed method involves solving the full AC power flow at each iteration. However, the power flow solution might not exist for a specific scenario, especially for a post-contingency situation. Furthermore, the proposed method suggests further increasing line loading which could lead to exceeding or operating close to the power transfer capability making the Jacobian matrix singular or ill-conditioned. If the power flow situation is infeasible, or the Jacobian matrix is ill-conditioned, auxiliary strategies must be employed to support convergence.

The solution we use is the following. If the power flow calculation does not converge, and the distribution factors cannot be obtained, the linear programming optimization is skipped. Instead, the APC of 10% of the current values is applied to all generators uniformly. This approach is applied every time a power flow calculation does not converge, until the AC power flow is successful. Starting with such a valid grid state, the method then is applied in a regular manner, and increases the generation according to the problem definition.

If the method still leads to a failed power flow, the next strategy is to specify a damping factor, that is applied to the difference between the previous LP solution and the latest LP solution. This approach reaches the solution slower, but avoids overshooting when the linearization through the DF deviates too much from the real system.

The inclusion of voltage constraints and current constraints also supports convergence by providing an additional envelope for the valid range of the generation set-points. The warm start of the AC power flow by initializing the voltage vector with the results of a valid power flow is also helpful to find a valid AC solution.

We also encountered an issue of oscillating solutions of the LP problem in certain scenarios. It is manifested by repeatedly switching between 2 solutions that have similar

TABLE IV  
COMPUTATION TIMES

Calculation	case5	case30	case118
PF	13.4 ms	8.31 ms	9.33 ms
TDPF	87.8 ms	54 ms	64 ms
LP-OPF	98 ms	1.41 s	247 ms
TDOPF	296 ms	4.29 s	3.43 s
SC-OPF	455 ms	18.6 s	468 s
SC-DTDOPF	6.98 s	361 s	733 s

overall costs but have different generator set-points. To address this issue, the bounds are shrunk halfway towards the latest solution after the LP problem was solved more than half of the maximum number of iterations, similarly to the approach suggested in [29]. In addition, choosing a slightly different set of costs for generators can help to avoid such oscillations. Furthermore, the change of the costs can be used as an additional criterion of convergence: if there is no convergence after a certain number of iterations but the total costs remain about the same, the procedure stops.

### VIII. COMPUTATION TIME

We compare computation times for three different power systems of different sizes: case 5, case 30, and case 118 [27], [30], [31]. The power system models were adjusted by setting the line type similarly to the example in the case study, and adding the relevant TDPF parameters. Furthermore, the maximum power limits of loads and generators were adjusted to cause violations of constraints. The loads have also been included as controllable elements. We created unrealistic consumption and generation scenarios to cause most ( $N-1$ ) situations to have violations of constraints, with the purpose of obtaining the calculation times.

For a large power system, such as case118, creating the LP problem for all the ( $N-1$ ) cases is not feasible because the arrays of the LP problem that include all the ( $N-1$ ) cases cannot be allocated in the available RAM. To address this issue, we add only those ( $N-1$ ) cases to the LP problem that have violations of constraints. In very large grids that have violations in a large number of ( $N-1$ ) cases this can still not solve this issue. The strategy for this case should be solving the LP optimization for the ( $N-0$ ) case first. If even after this step the number of ( $N-1$ ) cases with violations is too high, one should limit the number of ( $N-1$ ) cases that are included at the same time.

We can see from the Table IV that the computation time of the SC-DTDOPF is higher for larger grids. At the same time, the computation time does not necessarily depend on the size of the grid, but on the severity of the constraints violations. The performance of the calculation greatly depends on the number of iterations of the sequential method that are needed to achieve the solution, which in turn depends on the grid model and the constraint violations. For instance, the LP-OPF for case 30 system takes longer to converge than for the case 118 system.

### IX. DISCUSSION AND OUTLOOK

We developed and implemented a new method of SC-OPF that directly considers non-steady-state overhead power line temperature as a constraint —SC-DTDOPF. To this end, we use AC distribution factors from the inverted Jacobian matrix after a successful TDPF calculation. We demonstrated the benefits of curative APC in terms of the reduction of preventive APC in a case study of an example 5 bus system. We demonstrated that a shorter reaction time of curative APC leads to a higher reduction of preventive APC that is required in the ( $N-0$ ) operation.

Additional current limits besides the thermal limit must be considered, such as safety limits of other components of the power system. We included the elevated current limit (160%) as an additional constraint in the formulation of the LP problem. Consideration of the current limit in addition to the temperature limit is required for short reaction times to avoid exceeding the limits that are not related to line temperature. After a certain point, further reduction of the reaction time does not lead to an additional benefit of the reduction of APC, and the proposed method takes this effect into account.

Equipment of the TSO with reliable Information and Communication Technology (ICT) is an enabler for faster response times. If the presented approach is used by TSOs in planning and operation, it will lead to tangible benefits of a better grid utilization and lower OPEX. The specific configuration of the reaction time of curative APC should be evaluated based on the specific grid in a real life application. The value of the elevated current limit in practice depends on the existing equipment.

Our implementation can be improved to increase performance. Formulating the LP problem based on the Jacobian matrix and the admittance matrix directly rather than computing the distribution factors for the pandapower elements and mapping them to the pandapower tables would lead to better performance. The performance can be further improved by optimizing the creation of the Jacobian matrix. It can be rewritten to use numba or it can be written in C++.

An inclusion of the maximum amount of curative APC to satisfy the ramp constraints, as well as voltage control via reactive power, should be addressed in future work.

### X. ACKNOWLEDGMENTS

The authors thank Denis Mende, and Marco Pau from Fraunhofer IEE for their valuable suggestions. We thank Bonface Ngoko from Osaka University for answering our questions about the approximate temperature model.

The authors are solely responsible for the contents of this publication.

### XI. CONFLICT OF INTEREST

The authors declare no conflict of interests.

### XII. DATA AVAILABILITY STATEMENT

The data that support the findings of this study are described in sufficient detail to enable a reproduction of the results.

## REFERENCES

- [1] T. Bongers, J. Kellermann, M. Franz, and A. Moser, "Impact of curtailment of renewable energy sources on high voltage network expansion planning," in *2016 Power Systems Computation Conference (PSCC)*. IEEE, 2016, pp. 1–8.
- [2] P. Wiest, D. Groß, K. Rudion, and A. Probst, "Security-constrained dynamic curtailment method for renewable energy sources in grid planning," in *2017 IEEE PES Innovative Smart Grid Technologies Conference Europe (ISGT-Europe)*. IEEE, 2017, pp. 1–6.
- [3] J. Eickmann, C. Bredtmann, and A. Moser, "Security-constrained optimization framework for large-scale power systems including post-contingency remedial actions and inter-temporal constraints," in *Advances in Energy System Optimization*. Springer, 2017, pp. 47–63.
- [4] A. Hoffrichter, K. Kollenda, M. Schneider, and R. Puffer, "Simulation of curative congestion management in large-scale transmission grids," in *2019 54th International Universities Power Engineering Conference (UPEC)*, 2019, pp. 1–6.
- [5] K. Kollenda, A. Schrief, C. Biele, M. Lindner, N. Sundorf, A. Hoffrichter, A. Roehder, A. Moser, and C. Rehtanz, "Curative measures identification in congestion management exploiting temporary admissible thermal loading of overhead lines," *IET Generation, Transmission & Distribution*, vol. 16, p. 3171–3183, 2022.
- [6] R. Grünwald, "Moderne Stromnetze als Schlüsselement einer nachhaltigen Energieversorgung," Karlsruhe Institut für Technologie, Berlin, Tech. Rep., 2014. [Online]. Available: <https://www.tab-beim-bundestag.de/de/pdf/publikationen/berichte/TAB-Arbeitsbericht-ab162.pdf>
- [7] HAASE GmbH Österreich. (2021) Leiterseile aus Aluminium-Stahl (AL1 / ST1A) nach EN 50182:2001. [Online]. Available: <https://www.haase.at>
- [8] K. Heuck, K.-D. Dettmann, and D. Schulz, *Elektrische Energieversorgung*. Wiesbaden: Springer Fachmedien Wiesbaden, 2013.
- [9] IEEE Std. 738-2012, "IEEE standard for calculating the current-temperature of bare overhead conductors," Dec. 2013.
- [10] B. O. Ngoko, H. Sugihara, and T. Funaki, "Optimal power flow considering line-conductor temperature limits under high penetration of intermittent renewable energy sources," *International Journal of Electrical Power & Energy Systems*, vol. 101, pp. 255–267, 2018.
- [11] CIGRE Working Group 22.12, "Thermal behaviour of overhead conductors," Aug. 2002.
- [12] S. Frank, J. Sexauer, and S. Mohagheghi, "Temperature-dependent power flow," *IEEE Transactions on Power Systems*, vol. 28, no. 4, pp. 4007–4018, 2013.
- [13] J. Santos, A. G. Expósito, and F. P. Sánchez, "Assessment of conductor thermal models for grid studies," *IET generation, transmission & distribution*, vol. 1, no. 1, pp. 155–161, 2007.
- [14] A. Ahmed, F. J. S. McFadden, and R. Rayudu, "Weather-dependent power flow algorithm for accurate power system analysis under variable weather conditions," *IEEE Transactions on Power Systems*, vol. 34, no. 4, pp. 2719–2729, 2019.
- [15] B. Ngoko, H. Sugihara, and T. Funaki, "Validation of a simplified model for estimating overhead conductor temperatures under dynamic line ratings — comparison with the CIGRE model," *IEEE Transactions on Power and Energy*, vol. 138, no. 4, pp. 284–296, 2018.
- [16] R. D. Zimmerman and C. E. Murillo-Sánchez, "Matpower 6.0 user's manual," *Power Systems Engineering Research Center*, vol. 9, 2016.
- [17] B. Ngoko, H. Sugihara, and T. Funaki, "A temperature dependent power flow model considering overhead transmission line conductor thermal inertia characteristics," in *2019 IEEE International Conference on Environment and Electrical Engineering and 2019 IEEE Industrial and Commercial Power Systems Europe (EEEIC/I&CPS Europe)*. IEEE, 2019, pp. 1–6.
- [18] University of Kassel and Fraunhofer Institute for Energy Economics and Energy System Technology (IEE), "pandapower," <https://github.com/e2n1EE/pandapower>, 2022.
- [19] L. Thurner, A. Scheidler, F. Schafer, J. H. Menke, J. Dollichon, F. Meier, S. Meinecke, and M. Braun, "pandapower - an open source python tool for convenient modeling, analysis and optimization of electric power systems," *IEEE Transactions on Power Systems*, 2018. [Online]. Available: <https://arxiv.org/abs/1709.06743>
- [20] R. Bolgarny, G. Banerjee, D. Cronbach, S. Drauz, Z. Liu, M. Majidi, H. Maschke, Z. Wang, and L. Thurner, "Recent developments in open source simulation software pandapower and pandapipes," in *2022 Open Source Modelling and Simulation of Energy Systems (OSMSES)*, 2022, pp. 1–7.
- [21] R. Bolgarny, G. Banerjee, S. Meinecke, H. Maschke, F. Marten, M. Richter, Z. Liu, P. Lytaev, B. Alfakhouri, J. Kisse, and D. Lohmeier, "Open source simulation software pandapower and pandapipes: recent developments," in *2023 Open Source Modelling and Simulation of Energy Systems (OSMSES)*, 2023, pp. 1–7.
- [22] P. Wiest, "Probabilistische Verteilnetzplanung zur optimierten Integration flexibler dezentraler Erzeuger und Verbraucher," Ph.D. dissertation, Universität Stuttgart, 2018.
- [23] R. Bolgarny, Z. Wang, A. Scheidler, and M. Braun, "Active power curtailment in power system planning," *IEEE Open Access Journal of Power and Energy*, 2021.
- [24] P. Virtanen, R. Gommers, T. E. Oliphant, M. Haberland, T. Reddy, D. Cournapeau, E. Burovski, P. Peterson, W. Weckesser, J. Bright, S. J. van der Walt, M. Brett, J. Wilson, K. J. Millman, N. Mayorov, A. R. J. Nelson, E. Jones, R. Kern, E. Larson, C. J. Carey, Í. Polat, Y. Feng, E. W. Moore, J. VanderPlas, D. Laxalde, J. Perktold, R. Cimrman, I. Henriksen, E. A. Quintero, C. R. Harris, A. M. Archibald, A. H. Ribeiro, F. Pedregosa, P. van Mulbregt, and SciPy 1.0 Contributors, "SciPy 1.0: Fundamental Algorithms for Scientific Computing in Python," *Nature Methods*, vol. 17, pp. 261–272, 2020.
- [25] Q. Huangfu and J. J. Hall, "Parallelizing the dual revised simplex method," *Mathematical Programming Computation*, vol. 10, no. 1, pp. 119–142, 2018.
- [26] O. Alsac and B. Stott, "Optimal load flow with steady-state security," *IEEE Transactions on Power Apparatus and Systems*, vol. PAS-93, no. 3, pp. 745–751, 1974.
- [27] University of Kassel and Fraunhofer Institute for Energy Economics and Energy System Technology (IEE). (2022) Power system test cases. [Online]. Available: [https://pandapower.readthedocs.io/en/latest/networks/power\\_system\\_test\\_cases.html](https://pandapower.readthedocs.io/en/latest/networks/power_system_test_cases.html)
- [28] F. Li and R. Bo, "Small test systems for power system economic studies," in *IEEE PES General Meeting*, 2010, pp. 1–4.
- [29] K. R. C. Mamandur and R. D. Chenoweth, "Optimal control of reactive power flow for improvements in voltage profiles and for real power loss minimization," *IEEE Transactions on Power Apparatus and Systems*, vol. PAS-100, no. 7, pp. 3185–3194, 1981.
- [30] University of Illinois at Urbana-Champaign. (2022) Power cases. [Online]. Available: <https://labs.ece.uw.edu/pstca/>
- [31] University of Washington. (1999) Power system test case archive. [Online]. Available: <https://labs.ece.uw.edu/pstca/>